Available online at www.sciencedirect.com
ScienceDirect
Journal of Photochemistry and Photobiology A: Chemistry 182 (2006) 296–305
Journal of Photochemistry and Photobiology A:Chemistry
www.elsevier.com/locate/jphotochem

Improvement of efficiency of dye-sensitized solar cells based on analysis of equivalent circuit

Naoki Koide, Ashraful Islam *, Yasuo Chiba, Liyuan Han

Ecological Technology Development Center, Sharp Corporation, 282-1 Hajikami, Katsuragi, Nara 639-2198, Japan

Available online 5 May 2006

Abstract

The present paper discusses the principle of dye-sensitized solar cells (DSCs) in terms of a new physics-based equivalent circuit model. This model is proposed following analysis by electrochemical impedance spectroscopy of the voltage dependence of the internal resistance elements of DSCs. The influence of these elements upon cell performance in areas such as short circuit current density (J_{SC}), open circuit voltage (V_{OC}) and fill factor (FF) was examined based on the equivalent circuit. It was demonstrated that the haze factor of TiO_2 electrodes is a useful index when fabricating light-confined TiO_2 electrodes to improve J_{SC}, and that blocking the TiO_2 surface with molecules is an effective way of reducing interfacial charge recombination at the TiO_2 surface and of improving shunt resistance and V_{OC}. FF was also improved by reduction of the internal series resistance, which is composed of the following three elements: the redox reaction resistance at the platinum counter electrode, the resistance of carrier transport by ions in the electrolyte, and resistance due to the sheet resistance of the transparent conducting oxide. Finally, the highest efficiency scores of 10.4% and 10.8% (aperture illumination area 1.004 cm^2 and 0.2227 cm^2, respectively) were confirmed by a public test center.

Keywords: Dye-sensitized solar cell; Equivalent circuit; Haze factor; Internal resistance

1. Introduction

Much attention has been paid to the development of dye-sensitized solar cells (DSCs) during the past decade [1,2]. The principle of DSCs is considered similar to that of photosynthesis in a leaf, as, unlike in conventional solar cells, the light absorption and carrier transportation in DSCs occur separately. The process is thought to be as follows: electrons are injected from the photoexcited dye into the conduction band of the semiconductor oxide, from where they pass through the nanoparticles to the transparent conducting oxide (TCO) current collector and into the external circuit. The sensitizer is regenerated by electron transfer from a donor, typically iodide ions, which are dissolved in the electrolyte that is present in the porous semiconductor. The triiodide ions formed during the reaction diffuse to the counter electrode, where they are reduced back to iodide by the conduction band electrons that have passed though the external circuit that performs the electrical work. Although Grätzel and co-workers [3] report a DSC that uses a terpyridyl complex [Ru(tctpy)(NCS)$_3${$(C_4H_9)_4N$}$_3$ referred to as Black Dye] and that achieves a high efficiency of 10.4% as measured by the NREL public test center (USA), the efficiency of DSCs needs to be further improved for practical use as an alternative to conventional photovoltaic devices. Significant improvement is however rendered difficult by the mechanism of DSCs, which is not adequately understood, particularly from the physical viewpoint.

On the other hand, the electrical properties of conventional pn-junction solar cells have been analyzed using a simple equivalent circuit of the kind shown in Fig. 1. In this equivalent circuit, a series resistance (R_s) is in series with a diode that represents the electrical properties of the pn-junction, and a shunt resistance (R_{sh}) and a constant-current source (I_{ph}) are in parallel with the junction. The series resistance is mainly caused by the bulk resistance of semiconductor materials, metallic contacts, and interconnections, and the contact resistance between the metallic contacts and the semiconductor. The shunt resistance is due to leakage across the pn-junction around the edge of the cell, and the presence of crystal defects and/or impurities in the junction region. The source I_{ph} results from the excitation of excess carriers by solar radiation [4–6]. This equivalent circuit is a useful tool for understanding the output performance of solar cells and for improving cell performance in areas such as short-circuit current density (J_{SC}), open-circuit voltage (V_{OC}), R_s, R_{sh}

* Corresponding author. Tel.: +81 745 63 3539; fax: +81 745 63 3306.
E-mail address: ashraful.islam@sharp.co.jp (A. Islam).

1010-6030/$ – see front matter © 2006 Elsevier B.V. All rights reserved.
doi:10.1016/j.jphotochem.2006.04.030

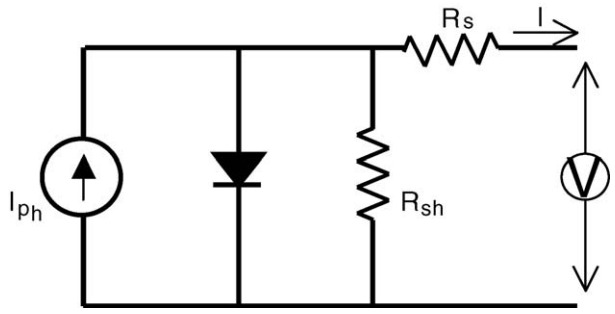

Fig. 1. Simple equivalent circuit model for conventional pn-junction solar cells. This model consists of a constant current source (I_{ph}), a diode, series resistance (R_s) and shunt resistance (R_{sh}).

and fill factor (FF) [4–6]. Analysis of DSCs thus requires study of a new equivalent circuit model, which may provide further information and allow a deeper comprehension of the electrical behavior of DSCs.

The present paper deals with the mechanism of DSCs from the physical viewpoint and, in Section 2, proposes a useful equivalent circuit for DSCs. Section 3 describes attempts to improve cell performance in areas such as J_{SC}, V_{OC} and FF based on analysis of the equivalent circuit. The current–voltage (I–V) characteristics with the confirmed highest efficiency for DSCs were also reported.

2. Modeling of equivalent circuit for dye-sensitized solar cells

2.1. Internal resistance analyzed by electrochemical impedance spectroscopy

Construction of theoretical models and performance simulations are necessary to improve the properties of DSCs. As with the modeling of conventional pn-junction solar cells, a number of approaches based on the continuity equation, the transport equation, and Poisson's equation have been attempted [7–17]. For example, Ferber et al. created performance simulation models in which electron transfer from TiO_2 to the oxidized ions was taken into account only as a recombination process [9–11]. Usami considered the recombination process from electrons in TiO_2 not only to oxidized ions in the electrolyte but also to oxidized dye on the electrodes [12–14]. Recently, Lee et al. reported on performance simulation models in which all the recombination processes that we can think of are considered based on the Marcus theory [16,17]. However, because the relation between the models and devices has not been clear, none of these efforts has led to an instructive and effective way of improving the efficiency of DSCs.

Meanwhile, electrochemical impedance spectroscopy (EIS) has been widely used to correlate device structure with a suitable model for the study of the kinetics of electrochemical and photoelectrochemical processes occurring in DSCs [18–30]. EIS is a well-known technique used for the study of electrochemical systems and its results are usually discussed in terms of equivalent circuits [18]. Boddy has proposed a number of equivalent circuits for the semiconductor–electrolyte interface consisting of combinations of resistors and capacitors [19]. It has also been found that the electrochemical properties of electrodes are strongly affected by their morphology [20–22]. These studies, unfortunately, discuss the electrochemical impedance of the TiO_2/dye/electrolyte interface from only one side, that is, under static conditions only. Moreover, since the experiments used DSCs with low energy conversion efficiency of less than 6%, they do not provide a useful approach for improving efficiency. More detailed EIS studies using stable and high-efficient DSCs have been required.

We therefore used DSCs with high energy conversion efficiency of over 8% to characterize the dependence of each internal resistance element on applied bias voltage [26]. Fig. 2 shows a typical Nyquist diagram of a DSC. Three semicircles are observed in the measured frequency range of 0.1 Hz–1 MHz. In our analysis, the three semicircles are attributed to the redox reaction at the platinum counter electrode (Z_1), the electron transfer at the TiO_2/dye/electrolyte interface (Z_2), and carrier transport by ions within the electrolyte (Z_3). The resistance elements R_1, R_2, and R_3 are described as the real part of Z_1, Z_2 and Z_3, respectively. It was found that the resistance element R_h in the high frequency range over 1 MHz is influenced by the sheet resistance of TCO and the contact resistance between the TCO and TiO_2. The former is the main factor in R_h, as the value of R_h increases in direct proportion to the sheet resistance of TCO.

2.2. Equivalent circuit for dye-sensitized solar cells

In general, solar cells must contain diode-like elements, but it is difficult to determine which impedance element displays diode-like behavior from EIS measurements under open circuit conditions. The I–V characteristics of a diode are given by

$$I = I_0 \left\{ \exp\left(\frac{qV}{nkT}\right) - 1 \right\}, \quad (1)$$

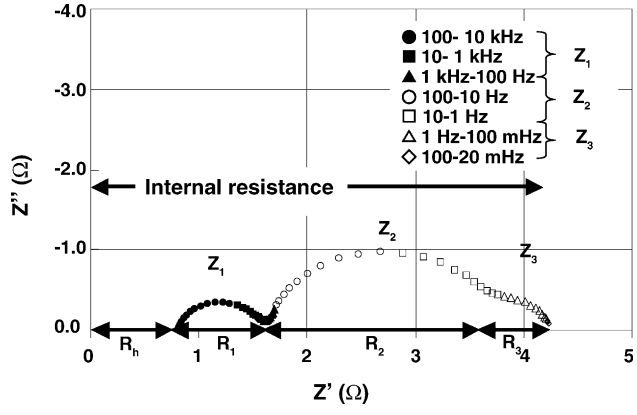

Fig. 2. Electrochemical impedance spectrum of a DSC. The three semicircular shapes are assigned to impedances related to charge transport at the Pt counter electrode (Z_1), at the TiO_2/dye/electrolyte interface (Z_2), and the carrier transport by ions within the electrolyte (Z_3), respectively. R_1, R_2 and R_3 are described as the real parts of Z_1, Z_2 and Z_3, respectively. R_h is defined as a resistance in the high-frequency range over 10^6 Hz.

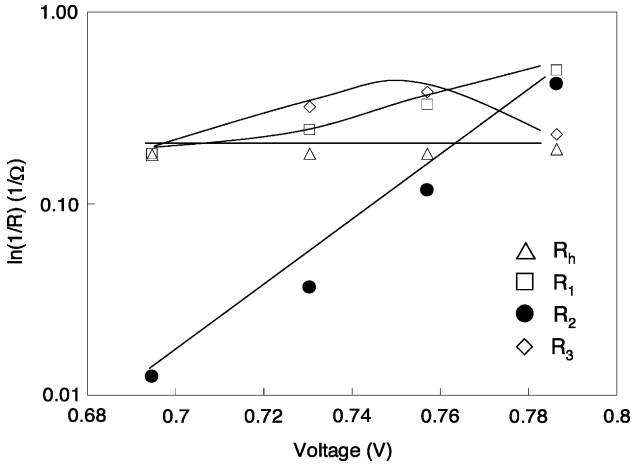

Fig. 3. Dependence of resistances R_h, R_1, R_2 and R_3 on the applied bias voltage. Measurement was carried out under V_{OC} by varying illumination conditions.

where I_0, q, V, n, k and T are diode saturation current, elementary charge, voltage, ideality factor, Boltzmann constant and temperature, respectively [4]. The resistance R is then described by

$$\frac{1}{R} \propto \exp\left(\frac{qV}{nkT}\right). \tag{2}$$

Since q, n, k and T are constants, $1/R$ should be proportional to the exponential function of V.

The dependence of R_h, R_1, R_2 and R_3 on the applied bias voltage at around V_{OC} was investigated. Fig. 3 shows the dependence of $1/R_h$, $1/R_1$, $1/R_2$ and $1/R_3$ on the applied bias voltage. It was found that $1/R_h$, $1/R_1$ and $1/R_3$ remain almost unchanged, while $\ln(1/R_2)$ increases in direct proportion to the applied bias voltage, which is consistent with Eq. (2). This result suggests that R_2 acts as a diode in DSCs, while R_h, R_1 and R_3 are series resistance elements.

From our experimental analysis by EIS, an equivalent circuit for DSCs was proposed as shown in Fig. 4. Z_2 functions to rectify the current and is represented as a diode. Here, a shunt resistance (R_{sh}) is added to the equivalent circuit to describe the back electron transfer across the TiO_2/dye/electrolyte junction mainly in the dye-free regions of the electrodes. However, R_{sh} cannot be determined from impedance spectrum. A straightforward method of estimating the shunt resistance from a DSC is to find the slope of the *I–V* curve at the short-circuit current point, which is typically of the order of $10^3\ \Omega\,cm^2$. Since the solar cells may have different areas, a common unit for resistance is $\Omega\,cm^2$. This area-normalized resistance is the result of replacing current with current density in Ohm's law. The equivalent circuit in Fig. 4 also has a constant-current source (I_{ph}), which describes the latent ability in J_{SC}.

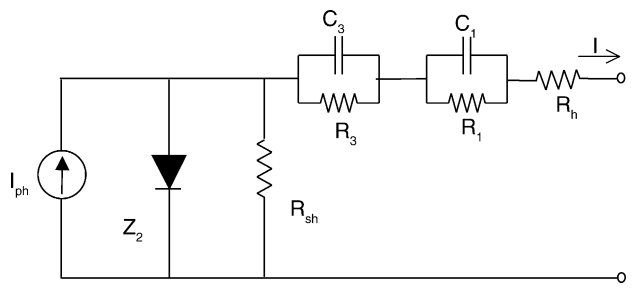

Fig. 4. Equivalent circuit model for DSCs. Z_2 functions to rectify the current and represented as a diode. The sum of R_1, R_3 and R_h largely corresponds to the series resistance of DSCs. A constant-current source I_{ph} and shunt resistance R_{sh} are in parallel with Z_2. C_1 and C_3 are capacitance elements of Z_1 and Z_3 (see Fig. 2), respectively.

In order to build up a clear image of the diode in the equivalent circuit, we would like to rewrite Eq. (1) in terms of electrochemistry. The Butler–Volmer equation [Eq. (3)] is well known as the Faradaic current by the electrode interface reaction [18].

$$i = -i_0\left\{\exp\left(\frac{-\alpha m FE}{RT}\right) - \exp\left(\frac{(1-\alpha)mFE}{RT}\right)\right\} \tag{3}$$

In Eq. (3), i_0 is exchange current, α the transfer coefficient ($0<\alpha<1$) which is one of the kinetic parameters of the electrode reaction, m is a stoichiometric number of electrons involved in the electrode reaction, F the Faraday constant which equals q times the Avogadro constant, E the electric potential at the electrode, and R is the gas constant which is defined as k times the Avogadro constant. Since electric potential E is much larger than $RT/(\alpha mF)$ under DSC operational conditions, Eq. (3) can be simplified to a Tafel equation as

$$i = i_0 \exp\left(\frac{(1-\alpha)mFE}{RT}\right) = i_0 \exp\left(\frac{(1-\alpha)mqE}{kT}\right) \tag{4}$$

If we assume Eqs. (5) and (6), (4) coincides with Eq. (1).

$$(1-\alpha)m = \frac{1}{n} \tag{5}$$

$$E = V \gg \frac{nkT}{q} \tag{6}$$

In other words, the Tafel equation is able to describe a rectifiable device like a diode, while the ideality factor of n in the diode is related with a stoichiometric number of electrons involved in the electrode reaction m and the transfer coefficient α. The rectification of the current is realized not only by use of a diode that is composed of a pn-junction but also by charge transfer at the interface of electrodes and solution. This fact strongly favors our equivalent circuit which had a diode at least around the maximum power point.

Comparison of the equivalent circuit for DSCs (Fig. 4) and conventional pn-junction solar cells (Fig. 1) shows that there is a difference only in series resistance. In the case of DSCs, series resistance is paralleled with two large capacitance elements, C_1 of the order of $10\ \mu F/cm^2$ and C_3 of the order of $1\ F/cm^2$ [26]. These capacitance elements bring a large time constant to the DSC. Hence, the *I–V* curves of DSCs are not accurately measured when using the same measurement conditions as for silicon solar cells as this large time constant causes slow response to applied bias in measurement. We have pointed out that correct measurement should be carried out with a prolonged delay time for measuring the current–voltage characteristics based on the equivalent circuit [31–33]. However, capacitance elements can be omitted since solar cells are generally operated under direct

current conditions. Consequently, R_s can be described as

$$R_s = R_h + R_1 + R_3. \quad (7)$$

We also confirmed that the R_s value of DSCs as estimated by EIS measurement using Eq. (7) is similar to that estimated from the slope of *I–V* measurement of DSCs.

Under direct current conditions, the equivalent circuit for DSCs is similar to that for conventional solar cells, although the mechanism is very different. This suggests that the accumulated experience gained through the development of high-efficiency conventional solar cells can be applied to DSCs. The cell performance can be divided into three parts, J_{SC}, V_{OC} and FF, as conversion efficiency corresponds to the product of these. The next section discusses the results of our attempts to improve cell performance based on analysis of the equivalent circuit for DSCs.

3. Strategy for raising efficiency

3.1. Improvement of J_{SC}

J_{SC}, which is described by a constant-current source in the equivalent circuit, can be calculated by integrating the product of an incident photon flux density ($F(\lambda)$) and the incident photon to the current efficiency (IPCE(λ)) of the cell over the wavelength (λ) of the incident light as in Eq. (8).

$$J_{SC} = \int qF(\lambda)(1 - r(\lambda))\mathrm{IPCE}(\lambda)\,\mathrm{d}\lambda, \quad (8)$$

where q is the electron charge, $F(\lambda)$ the incident photon flux density at wavelength λ, $r(\lambda)$ the incident light loss due to the light absorption and reflection by the conducting glass, and IPCE(λ) is defined as the incident monochromatic photon-to-electron conversion efficiency.

In the case of DSCs, light absorption occurs mainly at the photo-sensitive dye, as it is necessary to increase the IPCE of the photo-sensitive electrodes with dye. Therefore, IPCE is expressed as:

$$\mathrm{IPCE}(\lambda) = \mathrm{LHE}(\lambda)\phi_{e-inj}(\lambda)\eta_{CC}(\lambda) = \mathrm{LHE}(\lambda)\Phi(\lambda)_{ET} \quad (9)$$

where LHE(λ) is light-harvesting efficiency, $\phi_{e\text{-}inj}(\lambda)$ the electron injection yield from the dye excited state into TiO_2, $\eta_{CC}(\lambda)$ the charge collection efficiency at the front TCO electrodes and $\Phi(\lambda)_{ET}$ is defined as electron-transfer yield, that is, the product of electron injection yield and charge collection efficiency.

The values of $\phi_{e\text{-}inj}(\lambda)$ and $\eta_{CC}(\lambda)$ in DSCs have been examined by studies of electron transfer mechanism, for example transient absorption spectroscopy [34], and $\Phi(\lambda)_{ET}$ has been found to be close to 1 in high-efficiency DSCs [35–37]. It is therefore very important to increase LHE to improve short circuit current.

The LHE of the cell depends heavily on (1) the properties of the dye, such as extinction coefficient, absorbance and dye uptake on TiO_2 electrodes, and (2) the optical path length within the electrodes. Here we discuss the properties of the dye and optical path length within the electrode for the purpose of improvement of J_{SC}.

3.1.1. Development of sensitizer

Many dyes, including organic dyes [38–42] and transition metal complexes [1–3,43–54], have been employed in DSCs. One of the advantages of organic dyes is their high molar extinction coefficient. According to Hara et al., over 7% efficiency was achieved, which is nevertheless still lower than with the transition metal complexes based on Ru(II), Os(II), Pt(II), Fe(II), Re(I) and Cu(I) that have been developed for DSCs [53]. Of these, Ru(II)-based charge-transfer polypyridyl complexes show the highest energy conversion efficiency. This is because of their intense charge-transfer (CT) absorption in the whole visible range, moderately intense emission with fairly long lifetime in fluid solutions at ambient temperatures, high quantum yield for the formation of the lowest CT excited state, and redox reactivity and ease of tunability of redox properties. Photoexcitation of the metal-to-ligand charge-transfer (MLCT)-excited states of the adsorbed dye leads to an efficient injection of electrons into the conduction band of the TiO_2. IPCE values exceeding 70% have been reported in a number of cases.

The most efficient transition metal complexes employed so far in these solar cells are the Ru(II) bipyridyl complex $[Ru(dcbpy)_2(NCS)_2\{(C_4H_9)_4N\}_2$ referred to as N719] [2] and the terpyridyl complex $[Ru(tctpy)(NCS)_3\{(C_4H_9)_4N\}_3$ referred to as Black Dye] [3]. Of these two complexes, black dye has the higher J_{SC} value, with 21 mA/cm^2 against 17 mA/cm^2, because it absorbs light of longer wavelength. This suggests that J_{SC} could be improved by extending the dye absorbance to cover longer wavelengths.

The molecular design of new dyes that can absorb light up to the infrared wavelength region presents a challenging task in the further improvement of J_{SC}. Sugihara et al. reported an efficient Ru(II) 4,4′-dicarboxy-2,2′-bipyridine sensitizer containing one chelating β-diketonate ligand instead of two thiocyanate ligands [54]. The strong σ-donating nature of the negatively charged oxygen donor atom of the β-diketonato ligand destabilizes the ground state energy level of the dye, leading to lower energy shift of MLCT transitions compared to the thiocyanato-ruthenium(II) complex. In addition, the β-diketonato-ruthenium(II) sensitizer of Ru(4,4′,4″-tricarboxy-2,2′: 6′,2″-terpyridine) (β-diketonate)(NCS) with one NCS ligand shows efficient panchromatic sensitization of nanocrystalline TiO_2 solar cells [55]. Recently, we have developed a new β-diketonato Ru(II) complex, Ru (4,4′,4″-tricarboxy-2,2′: 6′,2″-terpyridine) (4,4,4-trifluoro-1-(4-fluorophenyl) butane-1,3-dione)(NCS) $\{(C_4H_9)_4N\}_2$, which shows very efficient panchromatic sensitization over the whole visible range extending into the near infrared region (ca. 950 nm) [56]. However, because of its lower V_{OC} compared to N719 and black dye, a conversion efficiency of 8.9% was attained under standard AM 1.5 irradiation (100 mW/cm^2) with J_{SC} of 20.4 mA/cm^2.

As mentioned above, although many dyes have been synthesized for improvement of performance, dyes with higher efficiency than black dye have not yet been developed.

3.1.2. Improvement of optical path length within TiO_2 electrode

Another approach to improvement of J_{SC} is to increase the optical path length in TiO_2 electrodes. The optical path length can be increased by the addition of relatively large particles to small particles to induce light scattering of the electrodes, which is also called the light-trapping effect. Usami theoretically points out that light-scattering magnitude in DSCs could be controlled by adding submicron particles to TiO_2 electrodes composed of nanocrystalline particles [57]. Most of the experimental work was concerned with rough estimation of the light-scattering magnitude from the LHE of the dye-adsorbed TiO_2 electrodes [36]. Grätzel and co-workers report that over 10% efficiency with N719 dye was achieved by using a TiO_2 electrode with double layers, one a transparent layer with particle size of about 20 nm and the other a scattering layer with particle size of 400 nm [58]. However, this high efficiency has not yet been reproduced by other groups, as the light-scattering effect is affected by certain subtle properties of the TiO_2 electrodes, such as the configuration of the TiO_2 particles, the distribution of particle size, the method of preparation of the electrode, and the sintering conditions.

Meanwhile, the concept of haze factor is well known as an index of TCO substrates for light scattering in the field of thin-film solar cells, such as amorphous silicon solar cells [59] and microcrystalline silicon solar cells [60,61]. In the relevant studies, an effective way of trapping light within the cell was found to be to increase the haze factor of the TCO substrates while controlling the surface morphology of TCO. Hence conversion efficiency can be improved by using a TCO with large haze factor due to the increase in the optical path length in the cells.

In the same manner, we have recently investigated the optical path length in DSCs using the haze factor of TiO_2 electrodes [62]. We also found that haze factor could be used as a suitable index for estimating the light scattering of TiO_2 electrodes in DSCs. Here, the haze factor of TiO_2 electrodes was defined as the ratio of diffused light to the total light transmitted through the electrodes.

In the case of DSCs, IPCE spectrum is primarily governed by the absorption spectrum of the dye. In general, IPCE in the long wavelength region is lower than in the short wavelength region because the extinction coefficient of the dye at longer wavelength is much lower. For example, black dye in ethanol has an extinction coefficient of about $7 \times 10^3\ mol^{-1}\ cm^{-1}$ at 620 nm, while extinction coefficient is about $200\ mol^{-1}\ cm^{-1}$ at 800 nm. Thus, although it is easy to make a DSC with black dye with IPCE of over 70% at 600 nm, IPCE at 800 nm is usually limited to 20%. For this reason, in order to raise cell efficiency to over 10%, it is necessary to increase the haze factor of the TiO_2 electrodes in the infrared wavelength region to increase the optical path length.

Fig. 5 shows the dependence of IPCE spectra on haze factors of 3–6% in TiO_2 electrodes at 800 nm. IPCE spectra at 800 nm increase enormously from 10% to 50% with increase in haze factor from 3% to 76%. On the other hand, IPCE spectra at around 600 nm increase gradually from 65% to ca. 80% with increase in haze factor from 3% to 53% and become saturated

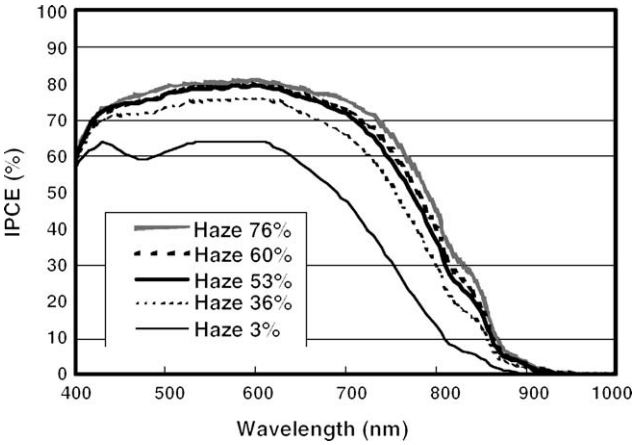

Fig. 5. The incident photon to current conversion efficiency (IPCE) of the DSCs using modified TiO_2 electrodes with different haze factor.

with further increase in haze factor. These results tell us that IPCE of 80% in the visible wavelength region is easily obtained using electrodes with medium haze factor because of the large extinction coefficient of the dye, while high IPCE in the infrared region demands high haze factor because of the small extinction coefficient of the dye.

Because J_{SC} is integral to IPCE over the sensitized wavelength region, the J_{SC} of DSCs will be improved with increase in haze factor especially in the infrared region using modified TiO_2 electrodes. Fig. 6 shows the dependence of J_{SC} on haze factor at 800 nm. We have demonstrated that J_{SC} increases in direct proportion to haze factor at 800 nm. The highest J_{SC} of $21\ mA/cm^2$ was achieved with haze factor of 76%. This result also indicates that the haze factor of the TiO_2 electrodes is a useful index for improving short circuit current in DSCs.

3.2. Improvement of V_{OC}

The total current through the cell is described in Eq. (10) from the analysis of the equivalent circuit in Fig. 1 [4]

$$I = I_{ph} - I_0 \left\{ \exp\left(\frac{q(V + IR_s)}{nkT} \right) - 1 \right\} - \frac{V + IR_s}{R_{sh}}. \qquad (10)$$

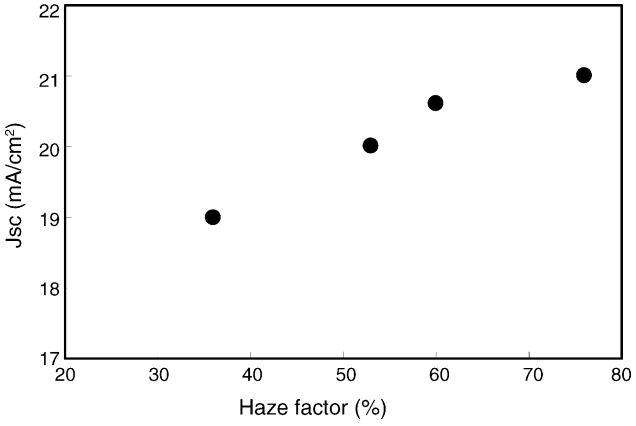

Fig. 6. Dependence of short circuit current density on haze at 800 nm.

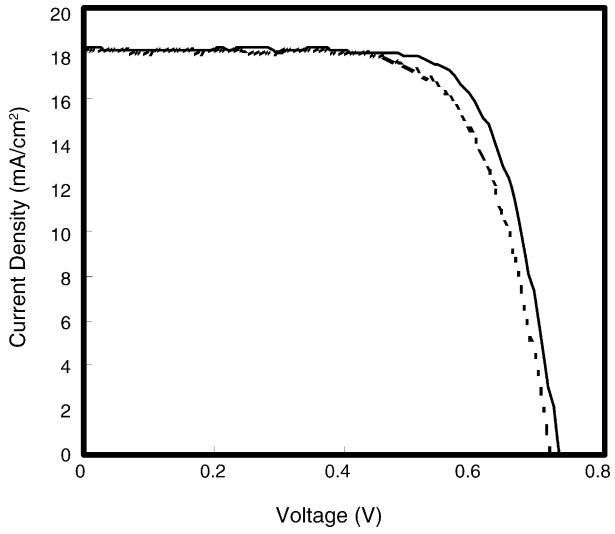

Fig. 7. Current–voltage characteristics of the DSCs with (closed line) and without (dashed line) THF in electrolyte.

Based on Eq. (10), V_{OC} is determined under conditions where the current source I_{ph} is equal to the sum of the current through the diode (I_d) (the second term on the right-hand side of the equation) and the current through the shunt resistance (I_{sh}) (the third term on the right-hand side of the equation). If we assume I_{ph} to be constant, I_0 in I_d and/or I_{sh} should be reduced for increase in V_{OC}.

The value of I_0 in the diode current of the equivalent circuit is strongly related to charge transfer at the TiO_2/dye/electrolyte interface in the reverse bias region, but since the mechanism of charge transfer in this region is still unclear, it is at present difficult to control I_0. Meanwhile, there have been many attempts to reduce I_{sh} by blocking the surface of TiO_2 with various molecules such as *tert*-butylpyridine (TBP) [2,3,8,63], alkylaminopyridine additives [64], combinations of acetic acid and methylpyrimidine or methylbenzimidazole [65], and pirimidine additives [66].

DSCs with TBP-treated dye-sensitized TiO_2 electrodes have high open circuit voltage because of the increased shunt resistance caused by blocking the TiO_2 surface with TBP molecules. For example, R_{sh} increases from 1 to 2 kΩ cm^2 with TBP treatment [63]. However, J_{SC} is unfortunately decreased by adding TBP to the electrolyte. It is well known that the conduction band of nanocrystalline TiO_2 electrodes depends on the pH of the electrolyte and that pyridine functions as a base within the electrolyte. Haque et al. [67] therefore concluded that the shift of the conduction band to more negative potentials results primarily from the interaction of TBP with dye-sensitized TiO_2 electrodes. This negative shift reduces the density of acceptor states available for electron injection and thereby retards the kinetics of electron injection. This is the main reason for the trade-off between V_{OC} and J_{SC} in DSCs with TBP. Recently, we have found an answer to this issue in THF molecules, which are effective in enhancing V_{OC} without loss of J_{SC}. The results are shown in Fig. 7 [68].

3.3. Improvement of FF

Resistive effects in solar cells reduce the efficiency of the solar cells by dissipating power in internal resistance. The key impact of internal resistance is to reduce FF [5]. As the fill factor is a measure of the "squareness" of the *I–V* curve, a solar cell with a higher voltage has a larger possible FF since the "rounded" portion of the *I–V* curve takes up less area. The maximum theoretical FF from a solar cell, described as the equivalent circuit in Fig. 1, can be determined by differentiating the power from a solar cell with respect to voltage and finding where this is equal to zero. Hence,

$$\frac{d(IV)}{dV} = 0 \tag{11}$$

giving

$$V_{mp} = V_{OC} - \frac{nkT}{q}\ln\left\{\left(\frac{qV_{mp}}{nkT}\right) + 1\right\}, \tag{12}$$

where V_{mp} is the voltage at the maximum power point. However, the above technique does not yield a simple or closed form equation. The equation above only relates V_{OC} to V_{mp}, and extra equations are needed to find FF. In the field of silicon solar cells, the more commonly used expression for FF can be shown empirically as

$$FF = \frac{v_{OC} - \ln(v_{OC} + 0.72)}{v_{OC} + 1}, \tag{13}$$

where v_{OC} is defined as normalized V_{OC}:

$$v_{OC} = \frac{q}{nkT}V_{OC}. \tag{14}$$

A key limitation of the equations described above is that they represent a maximum possible FF (which we called FF_0), although in practice FF will be lower due to the presence of internal resistive losses. For example, if values of $V_{OC} = 0.7$ V, $1 < n < 2$ and $T = 298$ K, typical values in the case of DSCs, are substituted in Eqs. (13) and (14), FF_0 is predicted to be from 0.75 to 0.85, whereas in practice FF is usually below 0.70. The effects of shunt and series resistance on FF in DSCs are explained in the following subsections.

3.3.1. Impact of shunt resistance

Low shunt resistance causes power losses in solar cells by providing an alternate current path for the light-generated current and lowers FF. An equation for FF as a function of shunt resistance can be expressed as below. The maximum power may be approximated as the power in the absence of shunt resistance minus the power lost in the shunt resistance. The equation for the maximum power from a solar cell then becomes

$$P'_{mp} = P_{mp}\left(1 - \frac{1}{r_{sh}}\right) \tag{15}$$

$$r_{sh} = \frac{R_{sh}}{R_{ch}} \tag{16}$$

$$R_{ch} = \frac{V_{mp}}{I_{mp}} \approx \frac{V_{OC}}{I_{SC}}, \tag{17}$$

where P'_{mp}, P_{mp}, r_{sh}, R_{ch}, V_{mp} and I_{mp} are the maximum power with shunt resistance, the maximum power in the absence of shunt resistance, normalized shunt resistance, characteristic resistance of the solar cell, voltage at the maximum power point, and current at the maximum power point, respectively [5]. Assuming that V_{OC} and I_{SC} are not affected by shunt resistance allows the effect of shunt resistance on FF to be determined as

$$FF = FF_0 \left(1 - \frac{1}{r_{sh}}\right), \tag{18}$$

where FF_0 is the fill factor in the case of infinite R_{sh}. It is predicted from Eqs. (16) to (18) that there is little room for improvement of FF (less than 1%) with increase of R_{sh}, as R_{sh} is of the order of $10^3\ \Omega\,cm^2$ and $1/r_{sh}$ is typically less than 1% in DSCs.

3.3.2. Impact of series resistance

The effect of series resistance on FF can be calculated in a manner similar to that used to find the impact of shunt resistance on FF. The equation which approximates the effect of series resistance on the output power of a solar cell then becomes

$$P'_{mp} = P_{mp}(1 - r_s) \tag{19}$$

$$r_s = \frac{R_s}{R_{ch}}, \tag{20}$$

where r_s is normalized series resistance [5]. Assuming that V_{OC} and J_{SC} are not affected by series resistance allows the impact of series resistance on FF to be determined by

$$FF = FF_0(1 - r_s). \tag{21}$$

In the above equation fill factor, which is not affected by series resistance, is denoted by FF_0.

These equations can be applied to all kinds of solar cells described by the equivalent circuit in Fig. 1. It is well known that FF increases with decreasing series resistance as in Eq. (21). In the case of DSCs, the series resistance is composed of the three resistance elements of R_1, R_3 and R_h as mentioned in Section 2 and the typical value of R_s is about $3\ \Omega\,cm^2$ as shown in Fig. 2. In other words, there is still room for improvement of up to about 10% in FF with decrease of R_s because the normalized series resistance r_s is about 0.1 in DSCs. Here, reduction of R_1, R_3 and R_h will be discussed in that order.

3.3.2.1. Series resistance R_1. Since R_1 is resistance related to charge-transfer processes occurring at the Pt counter electrodes, it should increase with increase in the surface area of the counter electrodes. In order to decrease R_1, we introduced a roughness factor (RF) as an index of the surface area of the counter electrodes. Here, RF is defined as the ratio of the total surface area to the projected area of the counter electrodes. The total surface area was measured by atomic force microscope (AFM) and the projected area was by optical microscope.

Counter electrodes with different roughness factors were prepared by depositing Pt thin film on glass substrates with different roughness factors. It was found that R_1 is inversely proportional to RF (Fig. 8). This result suggests that increase in the RF of the counter electrode leads to an accelerated rate of I_3^- reduction through the increased surface area of the counter electrode. In brief, R_1 can be decreased by $2\ \Omega\,cm^2$ by increasing the RF of the counter electrodes from 1.0 to 1.1.

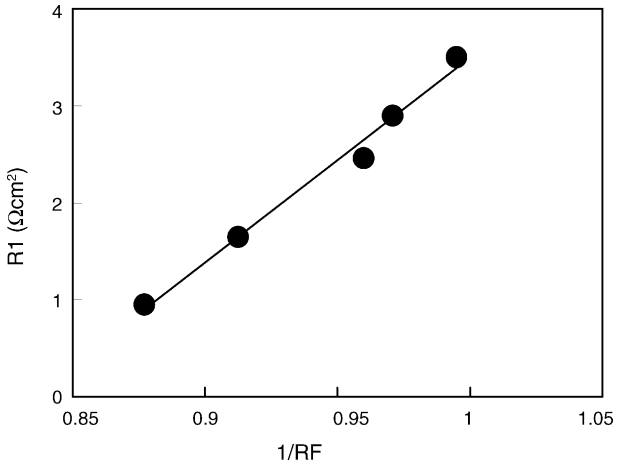

Fig. 8. Dependence of R_1 on roughness factor (RF) of the counter electrodes.

3.3.2.2. Series resistance R_3. R_3 is related to carrier transport by ions within the electrolyte. In order to decrease R_3, it is necessary to decrease the friction between two ions or between ions and solvent molecules in the electrolyte. We therefore used acetonitrile with low viscosity as the electrolyte solvent. In addition, to shorten the length of the electrolyte layer, the relationship between R_3 and the thickness of the electrolyte layer (d) was investigated (Fig. 9). This figure shows that cell performance can be improved by setting the counter electrode close to the TiO_2 film. The extrapolation of R_3 versus d data toward $d = 0$ gives a value of R_3 close to $0.7\ \Omega\,cm^2$. We consider this resistance to be related to the resistance of the electrolyte in the porous TiO_2 film, because the thickness is defined as the distance between the TiO_2 film and the counter electrode. Consequently, we can decrease R_3 to $0.7\ \Omega\,cm^2$ by decreasing d to zero.

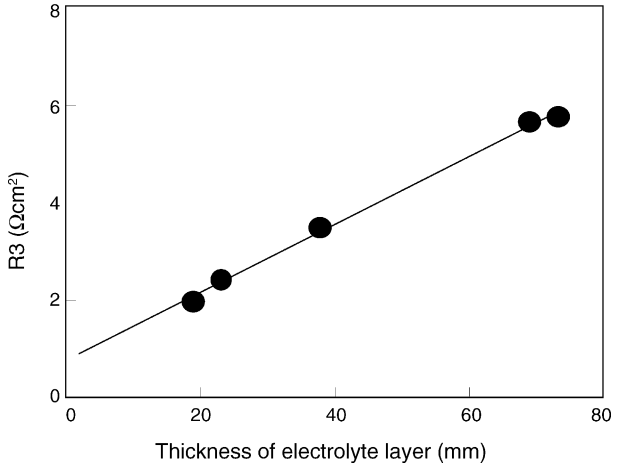

Fig. 9. Dependence of R_3 on thickness of electrolyte layer.

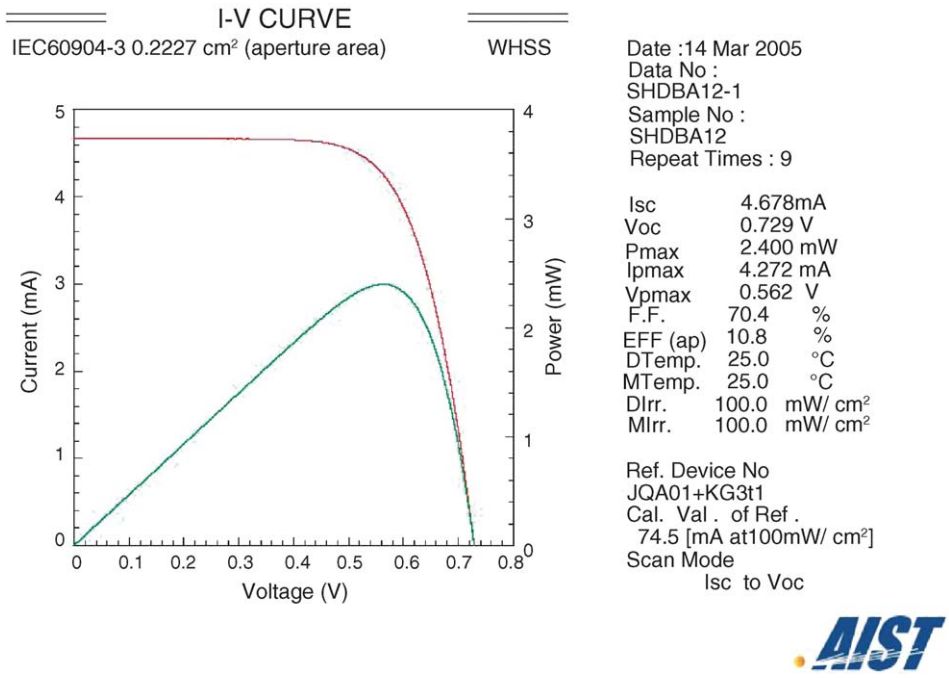

Fig. 10. Current–voltage characteristics of the DSC (aperture area 0.2227 cm^2).

3.3.2.3. Series resistance R_h. Finally, R_h, which is mainly attributed to the sheet resistance of the TCO substrates, should be discussed. It was also found that R_h increases in proportion to the increase in the sheet resistance of the TCO [69]. Although R_h could be theoretically reduced to 0 by using TCO with much lower sheet resistance, the efficiency of the cell would decrease due to decrease in the transmittance of the TCO. For example, while sheet resistance of 10 Ω/sq in the TCO, which is the norm in DSCs, gives R_h of about 1.0 Ω cm^2, sheet resistance of 5 Ω/sq reduces R_h to 0.5 Ω cm^2, but also reduces transmittance at wavelength of 600 nm from 83% to 78%. The optimum value for the sheet resistance of TCO is thought to be around 10 Ω/sq with transmittance of over 80% in the visible spectral region.

3.3.2.4. Total series resistance R_s. As mentioned above, by using a counter electrode with very large RF and TCO with very low sheet resistance, R_1 and R_h can be reduced to zero and R_3 to 0.7 Ω cm^2. The minimum series resistance is thus theoretically 0.7 Ω cm^2 when using acetonitrile solvent. However, the actual series resistance is much higher as it is not easy to produce

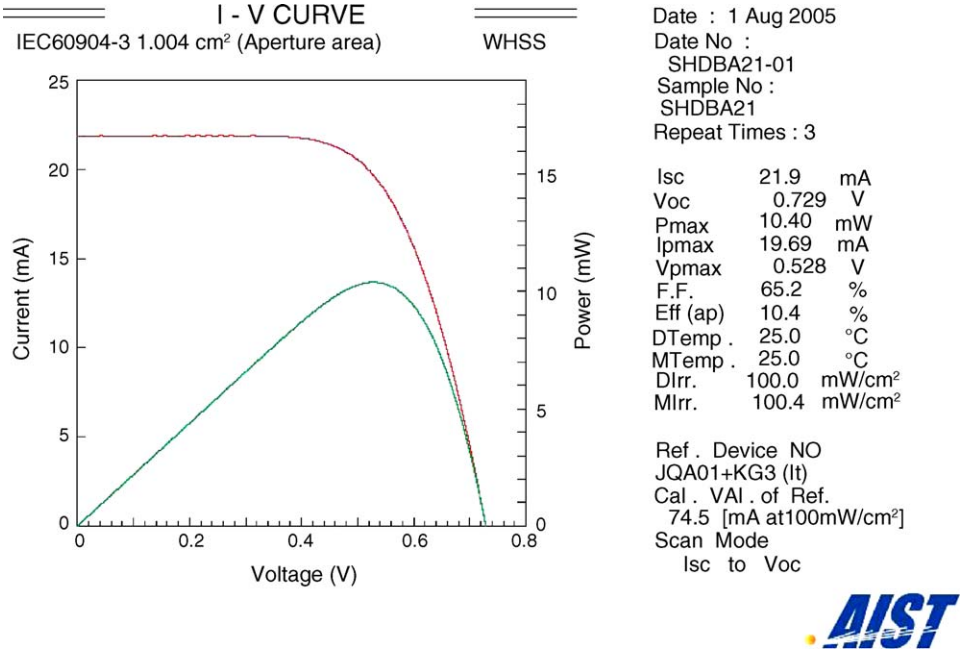

Fig. 11. Current–voltage characteristics of the DSC (aperture area 1.004 cm^2).

either a TCO substrate with both very low sheet resistance and high transmittance or a counter electrode with very large RF.

In order to improve conversion efficiency, TCO, the Pt counter electrode, and the thickness of the electrolyte layer were optimized simultaneously. After optimization, a cell with R_1 of 0.4 Ω cm^2, R_3 of 0.7 Ω cm^2 and R_h of 0.7 Ω cm^2 was fabricated, so that the total series resistance of the cell was successfully decreased from 2.7 to 1.8 Ω cm^2, which means that r_s decreases by 3%. It was found that FF is also improved by 3% by reducing r_s by 3%, which is consistent with Eq. (21) based on the equivalent circuit.

3.4. High-efficiency dye-sensitized solar cells

The cell performance of DSCs is optimized by control of J_{SC}, V_{OC} and FF as discussed above. In order to correctly evaluate the energy conversion efficiency [31–33], the *I–V* characteristics of the cells were also measured at the AIST public test center in Japan. Conversion efficiency of 10.8% at cell size of 0.2227 cm^2 and 10.4% at 1.004 cm^2 were finally achieved. The *I–V* curves of the high-efficiency DSCs are shown in Figs. 10 and 11, respectively.

In order to achieve a further large improvement in energy conversion efficiency, an understanding of the mechanism of DSCs must be fostered by analyzing charge transfer mechanisms as discussed in Section 2 and making every effort to improve J_{SC}, V_{OC} and FF as discussed in Section 3. The successful completion of future tasks—which include the development of a new sensitizer with an expanded wavelength region, suppression of recombination current in cells, the development of new redox species with more positive redox potential than I^-/I_3^-, the development of counter electrodes with very high RF, the development of a new electrolyte solvent with low viscosity, and the development of new TCO substrates with extremely low sheet resistance and high transmittance—will bring the energy conversion efficiency of DSCs up to the level of silicon solar cells.

4. Conclusions

In the present review, we discussed equivalent circuits for DSCs, which play an important role in the analysis and improvement of cell performance. It was found that the equivalent circuit for DSCs is similar to that for conventional solar cells except for the configuration of series resistance.

We successfully raised the energy conversion efficiency of DSCs through a strategy of improving the three parameters that determine cell performance. The haze factor of TiO_2 electrodes was found to be a useful index of increase in J_{SC}. It was also found that THF molecules could improve V_{OC} without loss of J_{SC}, and that FF was optimized by minimization of internal series resistance, that is, enlargement of the surface area of the counter electrodes, increase in the thinness of the electrolyte layer, and optimization of the sheet resistance of TCO.

As a result, the highest efficiency values of 10.4% and 10.8% (at aperture illumination areas of 1.004 and 0.2227 cm^2, respectively) were achieved.

Acknowledgements

Part of this work was supported by the New Energy and Industrial Technology Development Organization (NEDO) in association with the Ministry of Economy, Trade and Industry, Japan.

References

[1] B. O'Regan, M. Grätzel, Nature 353 (1991) 737.
[2] M.K. Nazeeruddin, A. Kay, I. Rodicio, R. Humphry-Baker, E. Müller, P. Liska, N. Valchopoulos, M. Grätzel, J. Am. Chem. Soc. 115 (1993) 6382.
[3] M.K. Nazeeruddin, P. Pechy, T. Renouard, S.M. Zakeeruddin, B. Humphry, P. Comte, P. Liska, L. Cevey, E. Costa, V. Shklover, L. Spiccia, G.B. Deacon, C.A. Bignozzi, M. Grätzel, J. Am. Chem. Soc. 123 (2001) 1613.
[4] See, for example;
S.M. Sze, Physics of Semiconductor Devices, Wiley, New York, 1981.
[5] M.A. Green, Solar Cells, vol. 96, Prentice-Hall, 1982, Chapter 5, p. 85.
[6] L. Castaner, S. Silvestre, Modelling Photovoltaic Systems using PSpice, John Wiley & Sons, Chichester, 2002, Chapter 3, p. 41.
[7] S. Soedergren, A. Hagfeldt, J. Olsson, S.-E. Lindquist, J. Phys. Chem. 98 (1994) 5552.
[8] S.Y. Huang, G. Schlichthoerl, A.J. Nozik, M. Grätzel, A.J. Frank, J. Phys. Chem. B 101 (1997) 2576.
[9] J. Ferber, R. Stangl, J. Luther, Sol. Energy Mater. Sol. Cells 53 (1998) 29.
[10] R. Stangl, J. Ferber, J. Luther, Sol. Energy Mater. Sol. Cells 54 (1998) 255.
[11] J. Ferber, J. Luther, J. Phys. Chem. B 105 (2001) 4895.
[12] A. Usami, Jpn. J. Appl. Phys. 36 (1997) L886.
[13] A. Usami, Chem. Phys. Lett. 292 (1998) 223.
[14] A. Usami, H. Ozaki, J. Phys. Chem. B 105 (2001) 4577.
[15] S. Tanaka, Jpn. J. Appl. Phys. 40 (2001) 97.
[16] J.-J. Lee, G.M. Coia, N.S. Lewis, J. Phys. Chem. B 108 (2004) 5269.
[17] J.-J. Lee, G.M. Coia, N.S. Lewis, J. Phys. Chem. B 108 (2004) 5282.
[18] See, for example;
A.J. Bard, L.R. Faulkner, Electrochemical Methods: Fundamentals and Applications, second ed., John Wiley & Sons, New York, 2001.
[19] P.J. Boddy, J. Electroanal. Chem. 10 (1965) 199.
[20] R.U.E. Lam, J. Schoonman, G. Blasse, B. Bunsenges, Phys. Chem. 85 (1981) 592.
[21] G. Nogami, Y. Ogawa, Y. Nishiyama, J. Electrochem. Soc. 135 (1988) 3008.
[22] E.J. Lee, S.I. Pyun, J. Appl. Electrochem. 22 (1992) 156.
[23] A. Hauch, A. Georg, Electrochim. Acta 46 (2001) 3457.
[24] R. Kern, R. Sastrawan, J. Ferber, R. Stangl, J. Luther, Electrochim. Acta 47 (2002) 4213.
[25] T. Hoshikawa, R. Kikuchi, K. Sasaki, K. Eguchi, Electrochemistry 70 (2002) 675.
[26] L. Han, N. Koide, Y. Chiba, T. Mitate, Appl. Phys. Lett. 84 (2004) 2433.
[27] M.C. Bernard, H. Cachet, P. Falaras, A. Hugot-Le Goff, M. Kalbac, I. Lukes, N.T. Oanh, T. Stergiopoulos, I. Arabatzis, J. Electrochem. Soc. 150 (2003) E155.
[28] M. Radecka, M. Wierzbicka, M. Rekas, Physica B 351 (2004) 121.
[29] F. F-Santiago, J. Bisquert, G. G-Belmonte, G. Boschloo, A. Hagfeldt, Sol. Energy Mater. Sol. Cells 87 (2005) 117.
[30] Q. Wand, J.-E. Moser, M. Grätzel, J. Phys. Chem. B 109 (2005) 14945.
[31] N. Koide, L. Han, Rev. Sci. Instrum. 75 (2004) 2828.
[32] N. Koide, Y. Chiba, L. Han, Jpn. J. Appl. Phys. 44 (2005) 4176.
[33] Y. Hishikawa, M. Yanagida, N. Koide, Proceedings of the 31st IEEE Photovoltaic Specialists Conference, Florida, 2005, p. 67.
[34] J.R. Durrant, S.A. Haque, E. Palomares, Coord. Chem. Rev. 248 (2004) 1247.

[35] J.S. Salafsky, W.H. Lubberhuizen, E. van Faassen, R.E.I. Schropp, J. Phys. Chem. B 102 (1998) 766.
[36] Y. Tachibana, H. Hara, K. Sayama, H. Arakawa, Chem. Mater. 14 (2002) 2527.
[37] R. Katoh, A. Furube, T. Yoshihara, K. Hara, G. Fujihashi, S. Takano, S. Murata, H. Arakawa, M. Tachiya, J. Phys. Chem. B 108 (2004) 4818.
[38] K. Hara, K. Sayama, Y. Ohga, A. Shinpo, S. Suga, H. Arakawa, Chem. Commun. (2001) 569.
[39] K. Hara, M. Kurashige, Y. Dan-oh, C. Kasasa, Y. Ohga, A. Shinpo, S. Suga, K. Sayama, H. Arakawa, N.J. Chem. 27 (2003) 783.
[40] K. Hara, M. Kurashige, S. Ito, C. Kasasa, A. Shinpo, S. Suga, K. Sayama, H. Arakawa, Chem. Commun. (2003) 252.
[41] K. Hara, Z.-S. Wang, T. Sato, A. Furube, R. Katoh, H. Sugihara, Y. Dan-oh, C. Kasada, A. Shinpo, S. Suga, J. Phys. Chem. B 109 (2005) 15476.
[42] T. Horiuchi, H. Miura, K. Sumioka, S. Uchida, J. Am. Chem. Soc. 126 (2004) 12218.
[43] R. Argazzi, C.A. Bignozzi, G.M. Hasselmann, G.J. Meyer, Inorg. Chem. 37 (1998) 4533.
[44] A. Islam, H. Sugihara, K. Hara, L.P. Singh, R. Katoh, M. Yanagida, Y. Takahashi, S. Murata, H. Arakawa, J. Photochem. Photobiol. A 145 (2001) 135.
[45] T. Renouard, R.-A. Fallahpour, Md. K. Nazeeruddin, R. Humphry-Baker, S.I. Gorelsky, A.B.P. Lever, M. Grätzel, Inorg. Chem. 41 (2002) 367.
[46] C. Klein, Md. K. Nazeeruddin, P. Liska, D.D. Censo, N. Hirata, E. Palomares, J.R. Durant, M. Grätzel, Inorg. Chem. 44 (2005) 178.
[47] Md. K. Nazeeruddin, S.M. Zakeeruddin, J.-J. Lagref, P. Liska, P. Comte, C. Barolo, G. Viscardi, K. Schenk, M. Grätzel, Coord. Chem. Rev. 248 (2004) 1317.
[48] G. Sauvé, M.E. Cass, G. Coia, S.J. Doig, I. Lauermann, K.E. Pomykal, N.S. Lewis, J. Phys. Chem. B 104 (2000) 6821.
[49] A. Islam, H. Sugihara, K. Hara, L.P. Singh, R. Katoh, M. Yanagida, Y. Takahashi, S. Murata, H. Arakawa, New J. Chem. 24 (2000) 343.
[50] A. Islam, H. Sugihara, K. Hara, L.P. Singh, R. Katoh, M. Yanagida, Y. Takahashi, S. Murata, H. Arakawa, G. Fujihashi, Inorg. Chem. 40 (2001) 5371.
[51] S. Ferrere, Chem. Mater. 12 (2000) 1083.
[52] G.M. Hasselmann, G.J. Meyer, Zeitschrift Physikalische Chemie Bd. 212 (1999) 39.
[53] N. Alonso-Vante, J. Nieregarten, J. Sauvage, J. Chem. Soc. Dalton Trans. (1994) 1649.
[54] H. Sugihara, S. Sano, T. Yamaguchi, M. Yanagida, T. Sato, Y. Abe, Y. Nagao, H. Arakawa, J. Photochem. Photobiol. A 166 (2004) 81.
[55] A. Islam, H. Sugihara, M. Yanagida, K. Hara, G. Fujihashi, Y. Tachibana, R. Katoh, S. Murata, H. Arakawa, New J. Chem. 26 (2002) 966.
[56] A. Islam, F.A. Chowdhury, Y. Chiba, R. Komiya, N. Fuke, N. Ikeda, L. Han, Chem. Lett. 34 (2005) 344.
[57] A. Usami, Sol. Energy Mater. Sol. Cells 64 (2000) 73.
[58] P. Wang, S.M. Zakkeruddin, P. Comte, R. Charvet, R. H-Baker, M. Grätzel, J. Phys. Chem. B 107 (2003) 14336.
[59] J. Meier, J. Spitznagel, U. Kroll, C. Bucher, S. Fay, T. Moriarty, A. Shah, Thin Solid Films 451–452 (2004) 518.
[60] Y. Zhao, S. Miyajima, Y. Ide, A. Yamada, M. Konagai, Jpn. J. Appl. Phys. 41 (2002) 6417.
[61] Y. Nasuno, M. Kondo, A. Matsuda, Jpn. J. Appl. Phys. 40 (2001) L303.
[62] Y. Chiba, A. Islam, K. Kakutani, R. Komiya, N. Koide, L. Han, Proceedings of the International Photovoltaic Science & Engineering Conference (PVSEC-15), Shanghai, 2005, p. 665.
[63] S.Y. Huang, G. Schlichthoerl, A.J. Nozik, M. Grätzel, A.J. Frank, J. Phys. Chem. B 101 (1997) 2576.
[64] H. Kusama, H. Arakawa, Sol. Energy Mater. Sol. Cells 81 (2004) 87.
[65] T. Kato, M. Fujimoto, T. Kado, S. Sakaguchi, D. Kosugi, R. Shiratuchi, W. Takashima, K. Kaneto, S. Hayase, J. Electrochem. Soc. 152 (2005) A1105.
[66] H. Kusama, H. Arakawa, J. Photochem. Photobiol. A 160 (2003) 171.
[67] S.A. Haque, E. Palomares, B.M. Cho, A.N.M. Green, N. Hirata, D.R. Klug, J.R. Durrant, J. Am. Chem. Soc. 127 (2005) 3456.
[68] A. Fukui, R. Komiya, R. Yamanaka, A. Islam, L. Han, Sol. Energy Mater. Sol. Cells 90 (2006) 649.
[69] L. Han, N. Koide, Y. Chiba, A. Islam, R. Komiya, N. Fuke, A. Fukui, R. Yamanaka, Appl. Phys. Lett. 86 (2005) 213501.